ATLAS Internal Note
PHYS-NO-051
22 December 1994

Search for $A/H \rightarrow \tau\tau$ decays

D. Cavalli, L. Cozzi, L. Perini, S. Resconi
Milano, 22/12/94

1 Introduction

This note follows closely the layout of the ATLAS Technical Proposal (TP) section on "Higgs sector in the MSSM" for what concerns the A/H$\rightarrow \tau\tau$ decays and expands it with more information on the points for which the authors think it is useful.
The main additions concern the e-μ channel analysis description, the p_T^{miss} resolution with different η coverages fully simulated until η=5, plots documenting most of the selection cuts used in the analysis, more information on the studies done at $10^{34}\ cm^{-2}s^{-1}$and various technical details.

2 Generalities

In the minimal supersymmetric extension of the Standard Model (MSSM), two Higgs doublets are required, resulting in 5 physical states, usually referred to as H^+, H^-, h (neutral lighter scalar), H (neutral heavier scalar) and A (neutral pseudoscalar). At the tree level their masses can be computed in terms of only two parameters, typically m_A and $tan\beta$ (the ratio of the vacuum expectation values of the two doublets). Radiative corrections [1] introduce a dependence on m_t: while the tree level relation $m_{H^+}^2 = m_A^2 + m_W^2$ is only slightly affected, the upper limit for m_h rises with m_t and with $m_{\tilde{q}}$; in particular the tree-level inequality $m_h < m_Z$ becomes $m_h < 125$ GeV for $m_t = 170$ GeV. Here the values $m_t = 170$ GeV and $m_{\tilde{q}} = 1$ TeV are assumed.
The parameter space of the MSSM, usually shown as extending over values $0 < m_A < 500$ GeV and $0 < tan\beta < 50$, can be explored through the A/H to $\tau\tau$ decays, which require very good τ-identification and E_T^{miss}-resolution.
These aspects of the ATLAS detector performance are described in section 3 and a full simulation of the detector performance was used to study as carefully as possible the sensitivity of the experiment to these decays.

Events have been generated with PYTHIA MC version 5.7 with the correct τ-polarisation inserted, and the event simulation has been done with GEANT 315 using

FLUKA (HADR=4) and DICE version 2.02 (maintained on the NEW disk from March 1994 until December 1994). The calorimeters are liquid argon calorimeters with a plate simulation of the Accordeon structure and the hadronic barrel and extended hadronic barrel are Tile calorimeters. The preshower is the separated RD3 preshower. A part of the simulation was done with the Cosener's House layout for the inner detector, a second part with the Panel layout: no appreciable differences were observed in the physical reconstructed quantities used in the following analysis. The collider energy is assumed $\sqrt{s} = 14$ TeV.
The simulation has been made with an η coverage of 3. The forward calorimeter region has been used at particle level, but the particle energies are smeared with $\frac{35\%}{\sqrt{E}} \oplus 4\%$ for em showers, and with $\frac{80\%}{\sqrt{E}} \oplus 7\%$ for hadronic ones, accordingly with the values of [2].

The integrated luminosity considered is $L = 10^4\ pb^{-1}$, which corresponds to one year running at a luminosity $\mathcal{L} = 10^{33}\ cm^{-2}\ s^{-1}$. In these conditions 1.8 minimum bias are foreseen to be superimposed to the good events. One minimum bias has been added to the simulated events: a check has been done adding 2 minimum bias events and no appreciable difference has been found in the reconstructed quantities interesting for our analysis. In the last section a study done for assessing the discovery potential of A/H$\rightarrow \tau\tau$ channel also at $10^{34}\ cm^{-2}s^{-1}$is described.

3 Detector performance

3.1 Reconstruction of p_T^{miss}

The invariant mass of a τ-pair can be reconstructed under the assumptions that $m_\tau = 0$, that the directions of the neutrino systems from each τ-decay coincide with that of the measured τ-decay products and under the condition that the τ-decay products are not back-to-back, which reduces considerably the acceptance for the signal [3].

If E_1, E_2 are the energies and $\overline{u_1}$, $\overline{u_2}$ the directions of the measured τ-decay products (electrons, muons or jets), and if p_x^{miss}, p_y^{miss} are the projections onto the x, y axes of the measured p_T^{miss}, then the energies E_{ν_1} and E_{ν_2} of the two neutrino systems from τ-decay can be obtained by resolving the system:

$$p_x^{miss}(p_y^{miss}) = (E_{\nu_1} * \overline{u_1})_{x,(y)} + (E_{\nu_2} * \overline{u_2})_{x,(y)}.$$

The measurement accuracy of p_x^{miss} and p_y^{miss} and the assumptions used result in many cases in unphysical negative solutions for E_{ν_1} and E_{ν_2}, for which the A-mass cannot be reconstructed.

A detailed evaluation of the p_T^{miss} resolution of the ATLAS detector has been performed. Particular attention was given to accurately inter-calibrate the various calorimeters (electromagnetic or $ECAL$ and hadronic or $HCAL$) and the preshower (PRE) detectors, and to evaluate non-linearities in response at low energy. The x and y components of p_T^{miss} were calculated from the transverse energies deposited in the cells with $|\eta| < 3$ and summed as:

$$E_T = \alpha \cdot {E_T}^{PRE} + \beta \cdot {E_T}^{ECAL} + \gamma \cdot {E_T}^{HCAL}$$

where 3 different sets of calibration constants α, β, γ were chosen for cells in an electromagnetic cluster, in a hadronic cluster and outside clusters. The first set was obtained minimising the difference between the nominal and reconstructed energy divided by the error for isolated electrons, the second one minimising the same quantity for hadronic jets. The last set was obtained minimising the difference between the total nominal energy in $|\eta|$ <3 and the total reconstructed energy in $|\eta|$ <3 divided by the error (parametrized as $\Delta E = 0.10 + 0.17 * E_{nom}$) in minimum bias events. In fact the distribution of the total reconstructed energy, using the jet calibration coefficients, divided by the nominal energy in $|\eta|$ <3 for a sample of minimum bias events was peaked at 0.91, so a third set of calibration constants was needed (the calibration constants for MB can be obtained multiplying the jet ones by the following factors: α by 1.2, β by 1.1 and γ by 1.1). The use of these calibration constants obtained from MB events for the reconstruction of energies of cells not belonging to a cluster (a cluster is built around a seed of E_T>1 GeV) is important for taking into account the non linearity of the calorimeter response to low energy particles [4].
An electronic noise with an RMS of 70 MeV per cell in the electromagnetic calorimeter and of 2.5 MeV per cell in the preshower was added at the cell level and only those cells with energy above 1.5 σ of noise were considered . The requirement used in the optimisation of this cut is the minimisation of both the difference between the reconstructed jet energies and the deterioration of the p_T^{miss} resolution with and without the noise added.
In the forward region, $3 < |\eta| < 5$, the contribution of the calorimeter resolution to the accuracy of the p_T^{miss} measurement is small and the computer time needed for full simulation very large, therefore the particles in this region were not fully simulated but their energies were appropriately smeared. This procedure was checked to be correct on a limited sample of events which were fully simulated over $|\eta| < 5$.

Figure 1 shows (for A mass= 200 GeV) the contribution to the p_x^{miss}, p_y^{miss}resolution for the different calorimeters regions, that is for the coverages $|\eta| < 1.4$, $1.4 < |\eta| < 3$, $3 < |\eta| < 5$. Each plot gives the difference between $\Sigma p_x(p_y)$ in the specified η range calculated at particle level and in full simulation; the fourth plot shows also the last range in full simulation (note the difference of statistics). It can be seen that the biggest contribution to p_x^{miss}, p_y^{miss}resolution comes from the barrel calorimeter, while the contribution of the forward calorimeter is small. Obviously this does not mean that the forward η coverage is not important, as it can be seen from Fig. 2, where the difference between p_x^{miss}calculated without η cut and with a cut at $|\eta| < 5$ or $|\eta| < 3$ at particle level is plotted.

Figure 3 shows the p_x^{miss}, p_y^{miss} resolution for the 4 simulated A masses, computed as difference between p_x^{miss}or p_y^{miss}calculated at particle level without η cut and p_x^{miss}or p_y^{miss}calculated with a coverage $|\eta| < 5$ (full simulation for $|\eta|$ <3 and appropriate smearing for $3 < |\eta| < 5$).

Figure 4 shows this p_x^{miss}, p_y^{miss} resolution as a function of the total transverse energy ΣE_T measured in the calorimeters (all the A events are used for this plot). This resolution is well described by the simple formula $0.46 \times \sqrt{\Sigma E_T}$ at a luminosity of $10^{33}\ cm^{-2}s^{-1}$.

The invariant mass of the τ-pair can then be reconstructed as:

$$m_{\tau\tau} = 2(E_1 + E_{\nu_1})(E_2 + E_{\nu_2})(1 - cos\theta),$$

where θ is the angle between the directions of the measured τ-decay products.
Figure 5 and Figure 6 show the different effects contributing to the width of the reconstructed $m_{\tau\tau}$ for m_A=150 GeV and m_A=300 GeV respectively. The first plot is the distribution of the $m_A$as generated by PYTHIA, the second plot gives the $m_{\tau\tau}$ reconstructed using in the above expression the quantities at particle level (here the p_T^{miss}components are calculated without η cut), the third plot is obtained in the same way of plot 2 using a cut $|\eta| < 5$ for the p_T^{miss}calculation, in the fourth plot the p_x^{miss} and p_y^{miss} obtained from the full simulation are used, finally in the fifth plot the reconstructed quantities also for the jet and the lepton are used. Note that the energy of τ-jet is reconstructed in the same way as the energy of all other jets: due to the large electromagnetic component in the τ-jet, its energy is overestimated of $\sim 5\%$; a correction of this effect would bring no significant improvement to the $m_{\tau\tau}$ reconstruction. A big effect in the width is seen already in the second plot, due to the assumption on the directions of the τ-decay products, the other big effect is seen in the fourth plot due to the p_T^{miss}resolution in full simulation (direction and module).

Figure 7 shows the distributions of the reconstructed $\tau\tau$ mass for m_A = 100, 150, 200 e 300 GeV respectively. The statistics is good because these plots are obtained after the cuts on E_T^{jet} and on $\Delta\phi(jet - \mu)$ described in section 4.1, without applying the τ-identification cut. The mass resolution increases from 12 to 36 GeV when m_A increases from 100 to 300 GeV.

3.2 τ-identification

The best sensitivity to the signal is achieved for events where one of the τ-leptons decays to hadrons (see section 4.1), but this sensitivity depends crucially on the quality of the τ-identification in the ATLAS detector, since backgrounds from jets are potentially very large. For this reason, a systematic study of τ-identification was performed, based on fully simulated $\tau \rightarrow$hadron decays and background events containing jets. A hadronic jet with $E_T > 40$ GeV and $|\eta| < 2.5$ was identified as a τ-jet if it satisfied the following criteria:

- $R_{em} < 0.07$, where R_{em} is the jet radius computed using only the e.m. cells contained in the jet;
- $\Delta E_T^{12} < 0.1$, where ΔE_T^{12} is the difference between the transverse energies contained in cones of size $\Delta R = 0.2$ and 0.1, normalised to the total jet transverse energy E_T;
- $N_{tr} = 1$, where N_{tr} is the number of reconstructed charged tracks with $p_T > 2$ GeV pointing to the cluster.

Figure 8 shows the distributions of these three quantities for the τ's from A (m_A=150 GeV) and for the jets from the $t\bar{t}$ background, all chosen with E_T>40 GeV. These distributions are done before any cut; however the 3 cuts are strongly correlated as it can be seen from Table 1 that shows the efficiencies of these criteria, computed sequentially, for hadronic τ-decays and for jets; separately b-jets and jets in $t\bar{t}$ or W+jets events

(the rejection of b-jets applying the τ-identification criteria is stronger than the rejection of other jets, also if it is computed with a large error: only 1 b-jet survives over 2000). The calorimeter cuts provide already a large rejection of $\sim$ 140 against jets with an efficiency of 28% for hadronic τ-decays. The ATLAS inner detector will be able (see section 3.8.5.2 of TP) to reconstruct all such tracks within a low-multiplicity jet environment with very high efficiency and negligible fake track rate, even at the highest luminosities expected at LHC. This cut provides an extra rejection factor of ~ 8 against jets at the expense of loosing the small fraction of 3-prong τ-decays in the signal sample.
The probability for a jet to satisfy the τ-identification criteria has been checked to be independent from the other kinematic cuts applied to the events, and is therefore used as a multiplicative acceptance factor in the results described in the next section, when the statistics is too low to apply all the cuts sequentially. In fact for all the backgrounds (except the Z^0 background) the rejection power of the cuts is so high that very few events (sometimes zero) would have survived after the direct application of all the kinematics and the τ-identification cuts. Thus the acceptance for the signals and the Z^0 background was calculated applying all the cuts, while for the other backgrounds the τ- identification cut is not applied sequentially, and it is taken as a multiplicative factor. A significant test has been done on the τ's from the A: applying all cuts sequentially or using the τ identification cut as a multiplicative acceptance factor gives results with a difference $\leq 10\%$.

4 Search for A/H$\rightarrow \tau\tau$ decays

The trigger for this channel is taken from the leptonic decay of one of the τ-leptons. The other τ-lepton may then decay to hadrons (lepton-hadron channel) or to another lepton (lepton-lepton channel). The lepton-hadron channel turns out to provide the best sensitivity to a possible A/H signal, mainly due to larger rate and to the more favourable kinematics of the τ-decay.

4.1 Lepton-hadron channel

The signal and background processes were generated with τ^--decays to muon and τ^+-decays to hadrons. They were fully simulated only for those events passing kinematic cuts ("filter cuts") which minimised the necessary computer time and did not bias the acceptance of the final cuts.

Signal:

$$pp \rightarrow A(H) + X$$
$$A(H) \rightarrow \tau^+\tau^-$$
$$\tau^+ \rightarrow had\ \bar{\nu_\tau}, \quad \tau^- \rightarrow \mu^-\bar{\nu}_\mu\nu_\tau$$

Backgrounds:

$$pp \rightarrow t\bar{t}$$

$$t \to W^+ b \quad \bar{t} \to W^- \bar{b}$$
$$W^- \to \mu^- \bar{\nu_\mu}, \quad W^+ \to \tau^+ \nu_\tau \quad \tau^+ \to had\ \bar{\nu_\tau} \tag{1a}$$
$$W^- \to \mu^- \bar{\nu_\mu}, \quad W^+ \to hadrons \tag{1b}$$

$$pp \to W^- + jets, \quad W^- \to \mu^- \bar{\nu_\mu} \tag{2}$$

$$pp \to b\bar{b}$$
$$b \to jets, \bar{b} \to \mu^- \tag{3}$$

$$pp \to Z^0 + X, \quad Z^0 \to \tau^+ \tau^-$$
$$\tau^+ \to had\ \bar{\nu_\tau}, \quad \tau^- \to \mu^- \bar{\nu_\mu} \nu_\tau \tag{4}$$

The charge conjugate decays as well as the processes with exchange e/μ were taken into account. The fraction of $A \to \tau\tau$ giving a final lepton-hadron state is 46%.

The $t\bar{t}$ background where one t decays to H^+ was also considered for low A masses (assuming m_{top}=170 GeV, m_{H^+} $\leq$160 GeV, that corresponds to m_A $\leq$140 GeV) and it was found to be negligible.
The numbers of events generated for signals and backgrounds are reported in Table 2 with the corresponding CPU times for one full simulated event and the description of the filter cuts applied after the generation at particle level before the full simulation of the detector.

In total 21637 events, stored in 113 3480-cartridges, have been fully simulated ($|\eta|$ <3) using a total of about 2500 hours of CPU (HP735/99 time).

The final kinematic cuts, which were applied to the reconstructed muon, jet and p_T^{miss} were chosen to be:
• ${p_T}^\mu > 24$ GeV and $|\eta|^\mu < 2.5$;
• Isolation of the trigger lepton, asking a $E_T < 5$ GeV in a window of half-width=0.6 centered around the lepton, which rejects leptons from $b\bar{b}$ by a factor 100 for a 90% efficiency for isolated leptons (see Figure 9);
• ${E_T}^{jet} > 40$ GeV, $|\eta|^{jet} < 2.5$;
• $1.8 < \Delta\phi^{jet-\mu} < 3.$ or $3.5 < \Delta\phi^{jet-\mu} < 4.5$;
• $\mathrm{m}_T(\mu - p_T^{miss}) < 25\ GeV$;
• $p_T^{miss} > 18$ GeV;
• $\mathrm{m}_{\tau\tau} = m_A \pm \Delta\mathrm{M}$.

Figure 9 and Figure 10 show the distributions of the most relevant quantities involved in kinematic cuts for signal and backgrounds: for each quantity, the distribution is shown for the signal and the background for which the cut on that quantity is more effective.
Figure 11 shows the reconstructed mass for the $t\bar{t}$ and $b\bar{b}$ backgrounds.
Assuming an additional 90% reconstruction efficiency for the trigger lepton, Table 3 shows the expected rates for the signal and the backgrounds within the chosen mass

bins, after all the above kinematical cuts. Table 4 shows details of the expected rates for all the backgrounds after applying also the efficiencies for τ-identification discussed in section 3.2. The background rates in Table 3 and 4 were obtained using the following production cross-sections [5]: $\sigma_{t\bar{t}} = 700\ pb$ for $m_t = 170\ GeV$, $\sigma_Z^0 = 46\ nb$, and taking $\sigma_{W+jets} = 16.8$ nb and $\sigma_{b\bar{b}} = 81$ nb (the values for σ_{W+jets} and $\sigma_{b\bar{b}}$ are cross sections asking for a μ with $p_T > 24$ GeV and $|\eta|^{jet} < 2.5$) [6].

For $m_A > 150$ GeV, m_A and m_H are very close and the signal cross-sections multiplied by the BR($\rightarrow \tau\tau$) for both Higgs bosons are comparable. The rates in Tables 3 to 5 therefore correspond to the summed A and H cross-sections. For $m_A = 100$ GeV however, $m_H \sim 140$ GeV and conservatively the H-signal alone was used, since the background from Z$\rightarrow \tau\tau$ decays is much larger than the A$\rightarrow \tau\tau$ signal.

Finally, Table 5 shows the expected rates and significances after all cuts, for a value of $tan\beta = 10$ and for an integrated luminosity of $10^4\ pb^{-1}$.

4.2 e-μ channel

The process

$$pp \rightarrow A(H) + X$$
$$A(H) \rightarrow \tau^+\tau^-$$
$$\tau^- \rightarrow \mu^-\bar{\nu_\mu}\nu_\tau,\ \tau^+ \rightarrow e^+\nu_e\bar{\nu_\tau} \qquad (1)$$

and its dominant backgrounds:

$$pp \rightarrow t\bar{t}$$
$$t \rightarrow W^+b,\ \bar{t} \rightarrow W^-\bar{b}$$
$$W^- \rightarrow \mu^-\bar{\nu_\mu},\ W^+ \rightarrow e^+\nu_e \qquad (2)$$

$$pp \rightarrow b\bar{b}$$
$$b \rightarrow ce^+\nu_e,\ \bar{b} \rightarrow c\mu^-\bar{\nu_\mu} \qquad (3)$$

were generated and fully simulated, together with the charge conjugate decays.
The fraction $A \rightarrow \tau\tau$ giving a final e-μ state is 6.3%.
The numbers of generated and simulated events for signals and backgrounds are lower than the numbers of Table 2. About 1300 events of signal (m_H=140 and m_A= 150, 200, 300 GeV) and about 500 events both for $t\bar{t}$ and $b\bar{b}$ backgrounds were fully simulated. The τ pair production via Drell-Yan or Z exchange followed by decay to e-μ, that is a significant background for A of 100 GeV mass, was not generated because, as in the previous section, the analysis on the H of 140 GeV mass is performed.

The kinematical cuts are:
- $p_{T_e}, p_{T_\mu} > 15\ GeV$, $|\ \eta_e\ |, |\ \eta_\mu\ | < 2.5\ GeV$
- isolation of the trigger leptons
- $|\ \sin\Delta\phi_{e,\mu}\ | > 0.2$
- $m_T(\mu - p_T^{miss}) < 40\ GeV$
- $p_T^{miss} > 15\ GeV$

• $m_{\tau\tau}$ is reconstructed and a cut is then applied in the same way as described in the previous section.

The dominant background for this channel for masses bigger than 140 GeV, is $t\bar{t}$; $b\bar{b}$ is suppressed by ϵ_{isol} on the two leptons, also if, due to the lower p_T cut for leptons, for a 90 % efficiency for the signal the rejection factor is 25.

The final results are reported in Table 6: the discovery potential at 5 σ is worse than the one obtained for the lepton-hadron channel. This is largely due to the fact that the cut on $m_T(\mu - p_T^{miss})$ is more effective for lepton -hadron, where this quantity for signal peaks at much lower values than for the e-μ cannel, as it can be seen comparing the distributions of Fig. 12 that are done for A mass= 200 GeV for the lepton-hadron and the $e-\mu$ channel respectively. There is also an effect due to the leptons from τ decay having a lower energy respect to the hadrons from τ due to the 3 body leptonic decay of the τ, as it can be seen in Fig. 13. Fig. 13 shows the comparison between the energy of jets from τ in the lepton-hadron channel and jets in $t\bar{t}$ background and the comparison between the energy of electrons from τ in the $e-\mu$ channel and electrons in $t\bar{t}$ background.

5 Discovery curve in (m_A, $tg\beta$) plane

Finally the curve (c) of Fig. 16 has been extracted as discussed in the previous sections for an integrated luminosity of 10^4 pb^{-1}. The final result is obtained imposing that the total significance, calculated summing the significances for the two channels in quadrature, exceeds the value of 5. This procedure is equivalent to compute the 5 standard deviation limit on σ_A (σ_5^{tot}) from the relation: $(\sigma_5^{tot})^{-2} = (\sigma_5^{l-h})^{-2} + (\sigma_5^{e-\mu})^{-2}$; therefore it is evident that the contribution of $e-\mu$ channel is rather marginal.
The values of $tan\beta$ above those of curve (c) correspond to larger production rates and couplings of the A/H to $\tau\tau$ pairs and the sensitivity to these decays would exceed 5 σ in this region.
For this channel there could be an ambiguity between SM and MSSM [1] only for masses $m_A \leq 100$ GeV and $tg\beta << 10$, that is in a region where ATLAS is not sensitive. It is interesting to note that for the other investigated channels, that give the other curves on Figure 16, ambiguities between SM and MSSM are also possible. In $h \to \gamma\gamma$, a h with mass of 70 GeV is produced with the same cross section for SM and MSSM with $tan\beta \sim 1$, while a h with mass of 110 GeV is the same approximately for $tan\beta \geq 30$. The same ambiguity can exist for $H \to \ell^+\ell^-\ell^+\ell^-$in the mass range $\sim 200 - 300$ GeV for $tan\beta << 2$.

6 High Luminosity

To evaluate the possibility to study the $A/H \to \tau\tau$ decays at high luminosity (10^{34} $cm^{-2}s^{-1}$), we have added the contribution due to the pile-up in the calorimeters at cell level. Our treatment is approximate: the pileup energy is assumed gaussian, the RMS is assumed constant in depth and the pileup contribution is added incoherently on all the cells. The RMS energy values due to the pile-up in calorimeters are taken from [8], appropriately rescaled for the different cells dimensions and luminosity used here. The RMS values:

40 MeV/$sin(\theta)$ per cell in the electromagnetic calorimeters and 180 MeV/$sin(\theta)$ per cell in the hadronic calorimeters have been used. With our assumptions, for an electromagnetic cluster 3×7 the average RMS due to the pileup turns out to be 317 MeV, in good agreement with the estimation reported in TP (section 2.7.1.1); for the hadronic calorimeter the evaluation of ref. [8] was done for the full LAr setup: in the barrel and extended barrel regions (Tile calorimeters) the pileup is expected to be smaller by a factor ∼4 [9] (the effect of this overestimation is discussed in the following). For the preshower an RMS value of 2.5 MeV/$sin(\theta)$ taken from [10] has been used. The electronic noise and the pile-up have been added incoherently in each cell. Only cells with an energy above 2.5σ of the total noise were considered (this cut was optimised in the same way described in section 3.1), while only cells with $E_T >$ 1.5 GeV were considered in the region $3 < |\eta| < 5$ covered by the Integrated Forward Calorimeter.
Figure 14 shows the p_T^{miss} resolution and the $m_{\tau\tau}$ reconstructed for m_A=150 GeV taking into account the full LAr pile-up energy; if the lower estimation is used instead for the Tile calorimeter, the RMS of the p_T^{miss} resolution of Fig. 14 is reduced by 15-20%.
Figure 15 shows the degradation of the p_T^{miss} resolution expected at a luminosity of $10^{34}\ cm^{-2}s^{-1}$, where the resolution is described by $1.1 \times \sqrt{\Sigma E_T}$, compared to the p_T^{miss} resolution at $10^{33}\ cm^{-2}s^{-1}$ already shown in Fig. 4.
The widening of the $m_{\tau\tau}$ distribution is a factor ∼1.4; however other aspects of the detector performance are affected by pile-up, in particular the quality of the τ-identification and the rejection power of the $m_T(\mu - p_T^{miss})$ cut. The total effect of the above 3 points has been estimated on the signal and on $t\bar{t}$ channel and gives a total increasing of a factor ∼3 for the background (no significant variation for the signal). So the complexive degradation on the significance is $\sqrt{3}$; a factor $\sqrt{1.4}$ is accounted for by the mass widening, leaving ∼1.4 as the evaluation of the remaining effects.

7 Conclusions

The main results of the study of the full simulated $A \rightarrow \tau\tau$ events are :

- the lepton-hadron channel has a bigger discovery potential than the $e-\mu$ channel
- the width of p_T^{miss} resolution depends strongly from the accuracy of the calorimeter calibrations and the effect of the electronic noise is small applying a threshold cut on the calorimeters cells
- with a τ-jet identification efficiency of 26% a rejection factor ∼ 400 against the jets and ∼ 2000 against the b-jets is reached
- the cut on the transverse mass of the system lepton-p_T^{miss} strongly reduces the $t\bar{t}$ background.

Due to the improvements in the 3 last points, the 5σ curve in the $(\tan\beta, m_A)$ plane that determines the discovery limit, obtained summing the results from the two channels, is better than the one (curve e) reported in Fig. 8.8 of [7]. The curve roughly covers the region between 100-300 GeV and $tg\beta > 10$.

References

[1] Z. Kunszt and F. Zwirner - Nucl. Phys. B385 (1992) 3

[2] Report of the ATLAS Review Panel on Forward Calorimetry, 1994

[3] R.K. Ellis et al. - Nucl. Phys. B297 (1988) 221
L. Di Lella - Aachen Proceeedings 2, 530

[4] D. Cavalli, L. Cozzi, L. Perini, P. Pronesti - ATLAS Internal Note PHYS-025 (1993)

[5] D. Froidevaux and E. Richter-Waas - ATLAS Internal Note PHYS-048 (1994)

[6] A. Nisati - Aachen Proceedings 3, 442

[7] ATLAS Letter of Intent

[8] P. Battaglia and L. Perini - ATLAS Internal Note CAL-018 (1993)

[9] M. Bosman - private communication

[10] A. Cravero and F. Gianotti - ATLAS Internal Note CAL-031 (1993)

Table 1: *Efficiency of τ-identification criteria described in text for hadronic τ-decays and for jet backgrounds.*

Cuts	A$\rightarrow \tau\tau$	b-jets	Other jets
R_{em}	43%	0.8%	1.2%
ΔE_T^{12}	28%	0.4%	0.7%
N_{tr}	26%	0.05%	0.25%

Table 2: *Statistics used*

Events	n^0events generated	n^0events detector simulated	sim. time 1 ev. (s) HP735/99	filter cuts
m_A= 100 GeV	50400	3135	~290	$p_T{}^{\mu} > 24$ GeV and $\|\eta\|^{\mu} < 2.5$
$m(H)$= 140 GeV	10419	1866	~320	$E_T{}^{h_\tau} > 30$ GeV and $\|\eta\|^{h_\tau} < 2.5$
m_A= 150 GeV	10800	2170	~335	(where $\tau \rightarrow h_\tau \nu_{tau}$)
m_A= 200 GeV	4265	1855	~370	
m_A= 300 GeV	1900	952	~500	
$Z \rightarrow \tau\tau$	89200	2339	~140	
$t\bar{t}$ ($\rightarrow W \rightarrow jets$)	6784	1108	~430	$p_T{}^{\mu} > 24$ GeV and $\|\eta\|^{\mu} < 2.5$
$t\bar{t}$ ($\rightarrow W \rightarrow \tau$)	11458	2210	~510	$m_T(\mu - p_T^{miss}) < 50\ GeV$
W+jets	197246	3819	~220	$p_T{}^{\mu} > 24$ GeV and $\|\eta\|^{\mu} < 2.5$ $m_T(\mu - p_T^{miss}) < 50\ GeV$ at least 1 string with $p_T > 30$ GeV
$b\bar{b}$	929440	2183	~400	$p_T{}^{\mu} > 24$ GeV and $\|\eta\|^{\mu} < 2.5$ $\hat{p_T} > 15 GeV$

Table 3: *For an integrated luminosity of* 10^4 pb^{-1}, *expected signal and background rates after kinematic cuts for the lepton-hadron A/H*$\rightarrow \tau\tau$ *channel.*

Signal mass (GeV)	$m_H = 140$	$m_A = 150$	$m_A = 200$	$m_A = 300$
Mass bin (GeV)	115-165	120-180	170-230	245-355
σ for $tan\beta = 10$(pb)	2.91	4.48	1.59	0.35
Signal for $tan\beta = 10$	261	487	414	124
W + jets	23360	35040	38050	58410
$t\bar{t}$ ($\rightarrow W \rightarrow$ jets)	7190	9910	13800	16680
$t\bar{t}$ ($\rightarrow W \rightarrow \tau$)	490	660	660	790
$b\bar{b}$	133580	140270	72520	66780
Z$\rightarrow \tau\tau$	1280	660	170	-

Table 4: *For an integrated luminosity of* 10^4 pb^{-1}, *expected background rates after all cuts for the lepton-hadron A/H*$\rightarrow \tau\tau$ *channel*

Signal mass (GeV)	$m_H = 140$	$m_A = 150$	$m_A = 200$	$m_A = 300$
W+jets	56 ± 23	83 ± 31	91 ± 32	140 ± 44
$t\bar{t}$ ($\rightarrow W \rightarrow$ jets)	17 ± 4	24 ± 6	33 ± 8.1	40 ± 10
$t\bar{t}$ ($\rightarrow W \rightarrow \tau$)	3 ± 1	4 ± 1	4 ± 1	5 ± 2
$b\bar{b}$	64 ± 64	68 ± 68	35 ± 35	32 ± 32
Z^0	63 ± 63	44 ± 53	17 ± 33	-
Total	203 ± 94	223 ± 91	180 ± 59	217 ± 56

Table 5: *For an integrated luminosity of* 10^4 pb^{-1}, *expected rates and significances for the lepton-hadron* $A/H \rightarrow \tau\tau$ *channel.*

Signal mass (GeV)	$m_H = 140$	$m_A = 150$	$m_A = 200$	$m_A = 300$
Mass bin (GeV)	115-165	120-180	170-230	245-355
Acceptance signal (%)	0.6	0.7	1.6	2.6
Signal $tan\beta = 10$	65	109	96	35
Total background	200 ± 90	220 ± 90	180 ± 60	220 ± 60
Significance	4.1	7.3	7.3	2.3
5σ limit on σ_A	3.2 ± 1.5	2.8 ± 1.2	1.0 ± 0.4	0.8 ± 0.2
5σ limit on $tan\beta$	10.7 ± 4.0	8.9 ± 2.0	8.7 ± 1.2	15.1 ± 2.0

Table 6: *For an integrated luminosity of* 10^4 pb^{-1}, *expected rates and significances,* $e - \mu$ *channel*

	H 140	A 150	A 200	A 300
Acc signal (%)	6.6	7.9	8.9	14.
t $\overline{t}$ backg	2348±426	2582±447	1252 ± 312	1956±389
b $\overline{b}$ backg	693±282	1040±344	231 ± 163	231±163
tot backg	3041 ± 511	3623±564	1483±352	2187±422
5σ limit on σ_A	10.1±2.0	9.1±1.5	5.2±1.3	4.1±0.9
5σ limit on $tan\beta$	20.2±2.0	15.4±1.2	18.8±2.2	36.5±3.5

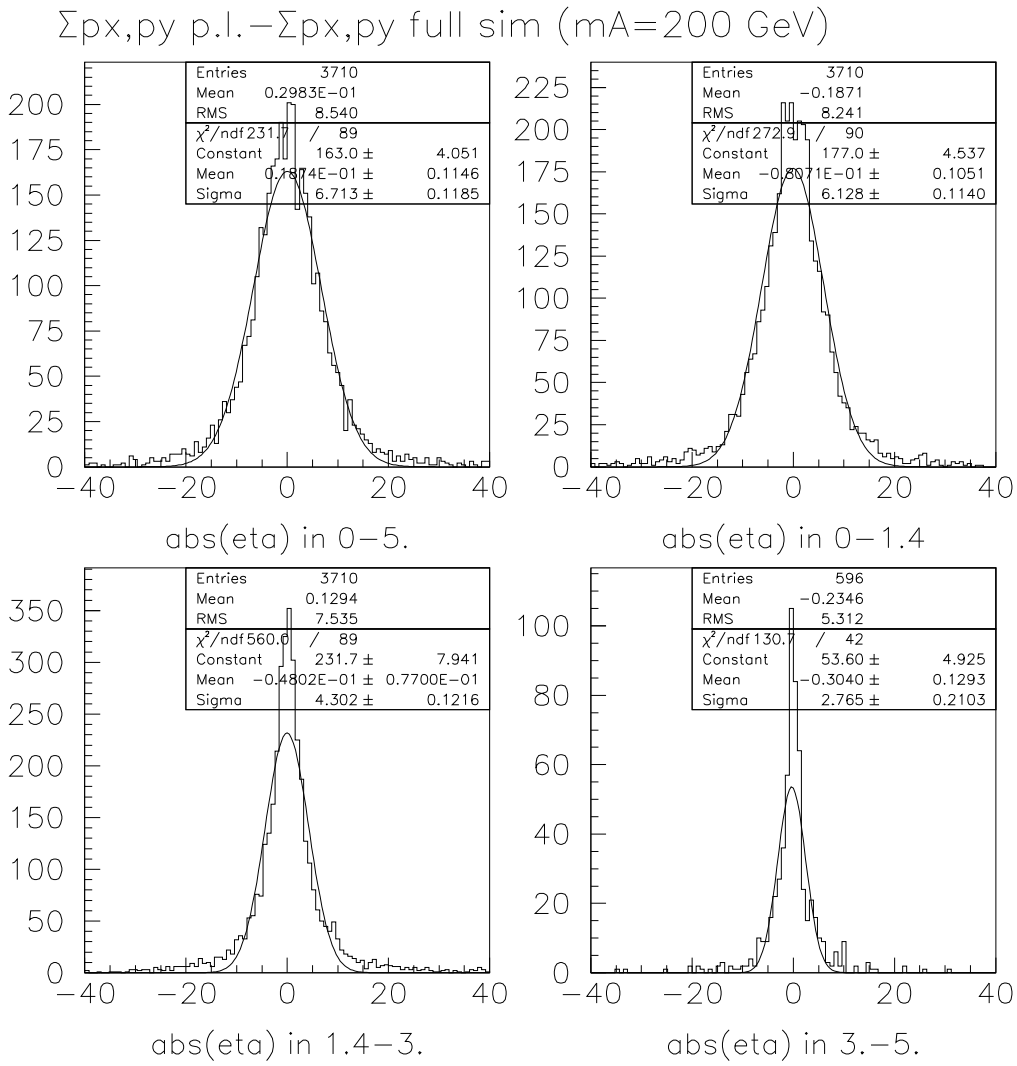

Figure 1: *Contributions to the p_x^{miss}, p_y^{miss} resolution from different parts of the calorimeter.*

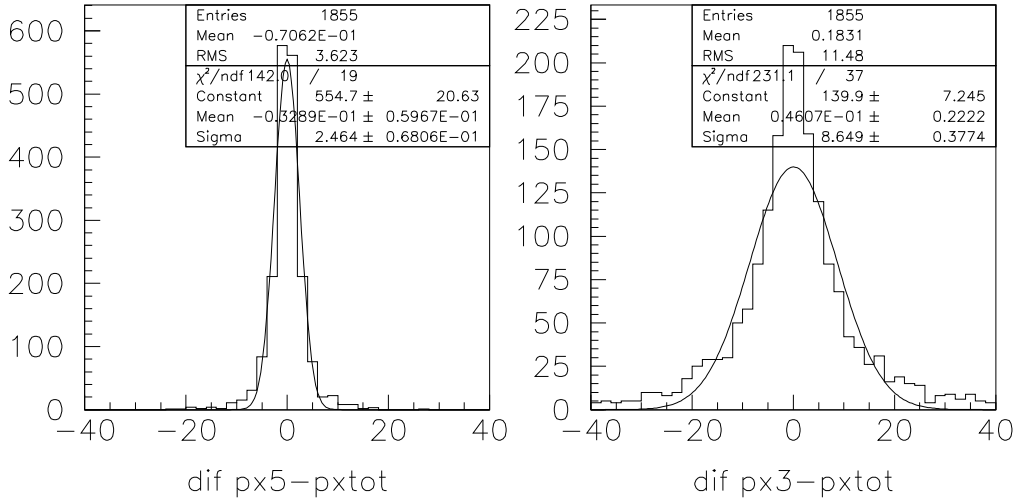

Figure 2: *Particle level p_x^{miss}, p_y^{miss} resolution for different η coverages: difference between p_x^{miss} calculated without η cut and with a cut $|\eta| < 5.$ or $|\eta| < 3.$ at particle level.*

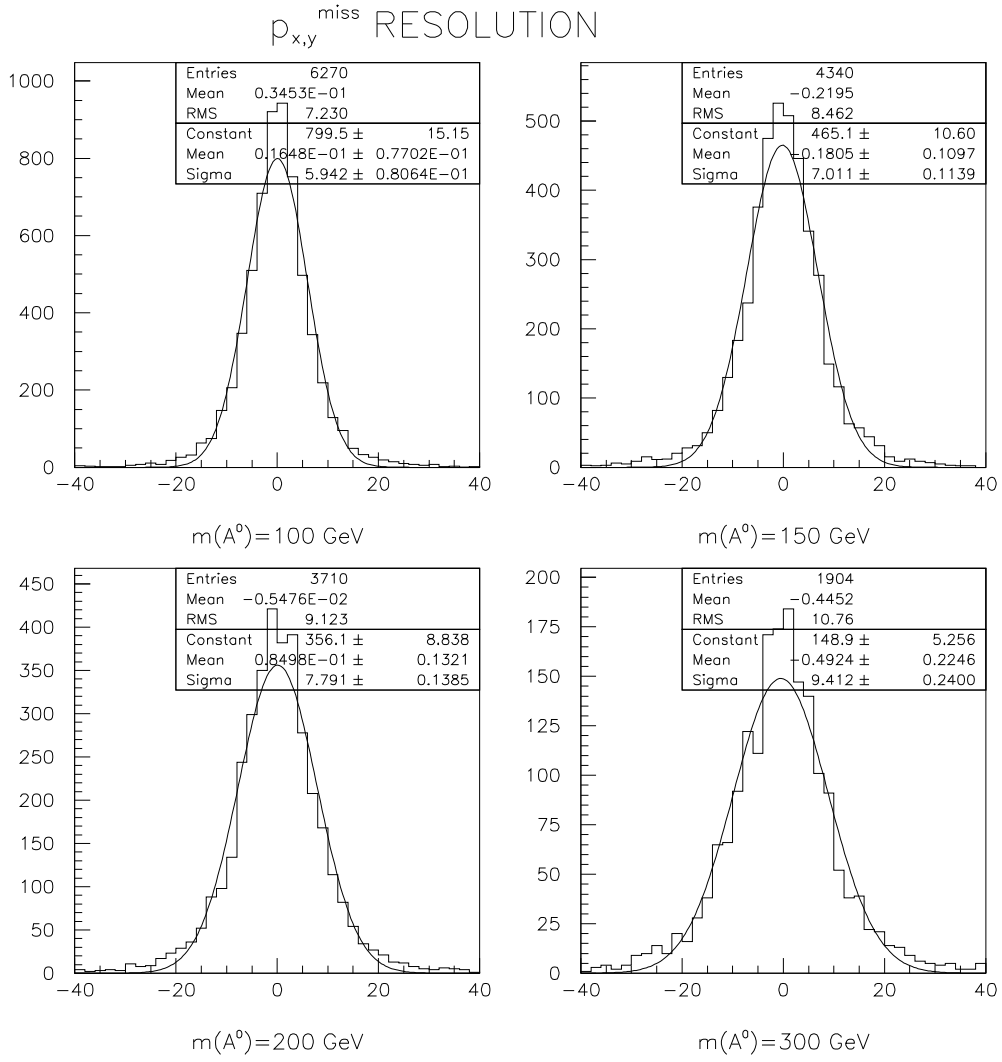

Figure 3: $p_{x,y}^{miss}$ *resolution for the 4 simulated A masses.*

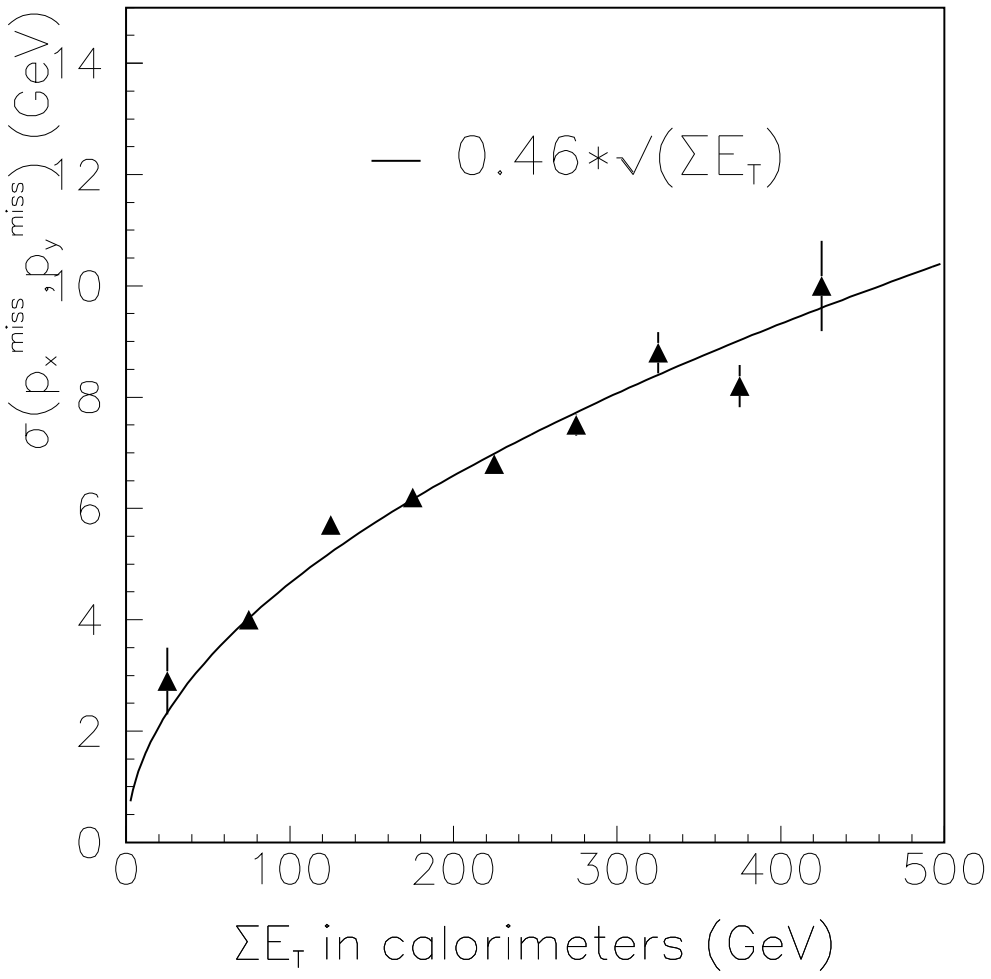

Figure 4: *ATLAS detector p_T^{miss} resolution vs ΣE_T at a luminosity of* $10^{33}\ cm^{-2}s^{-1}$.

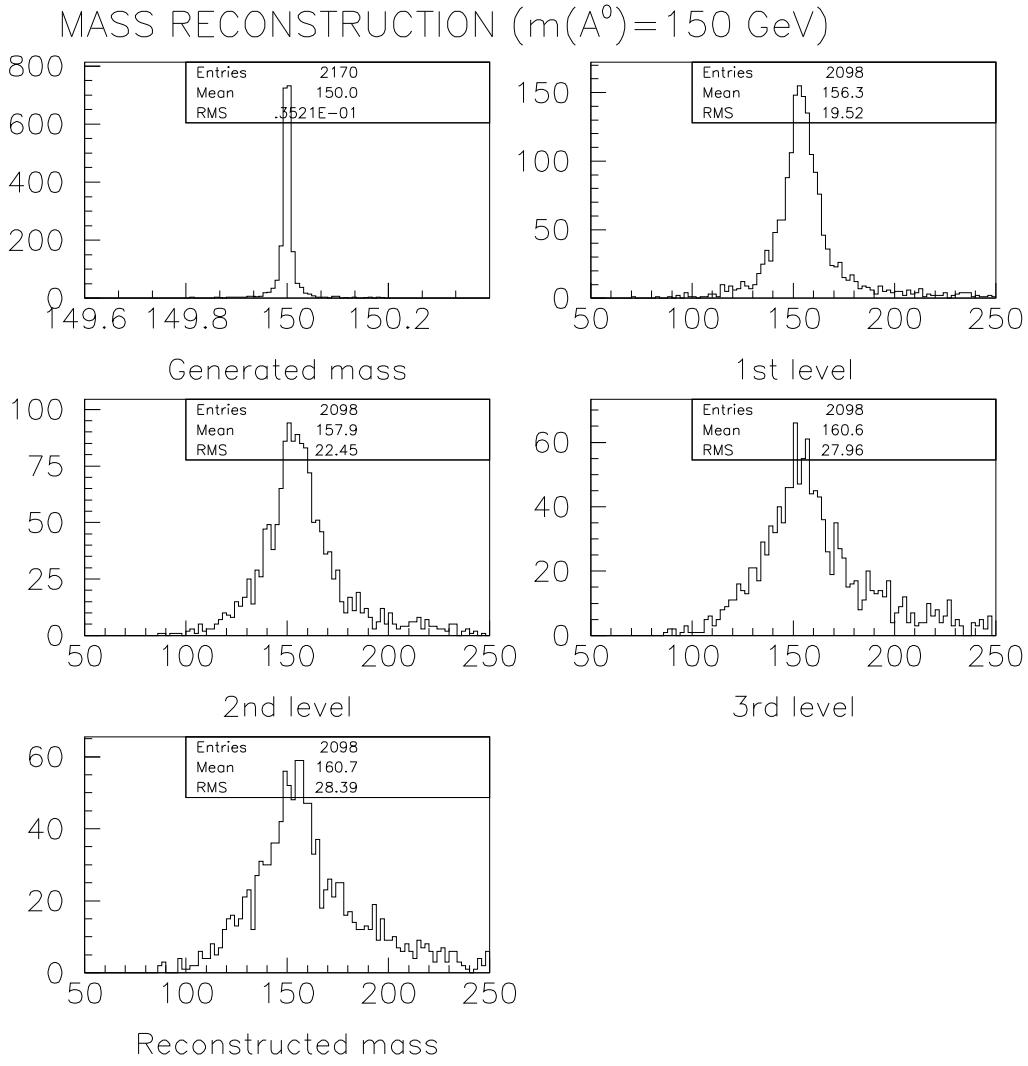

Figure 5: *Different effects contributing to the reconstructed $m_{\tau\tau}$ resolution, m_A=150 GeV.*

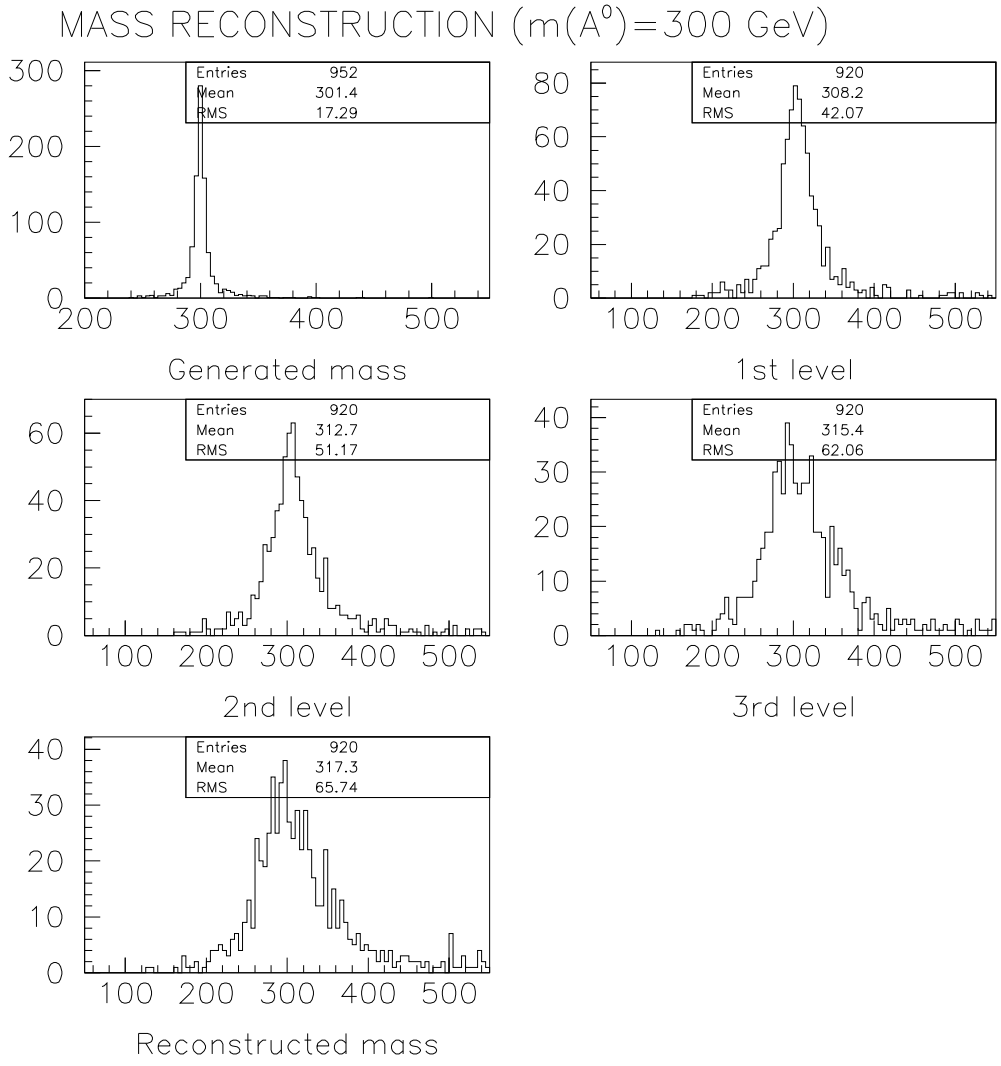

Figure 6: *Different effects contributing to the reconstructed $m_{\tau\tau}$ resolution, m_A=300 GeV.*

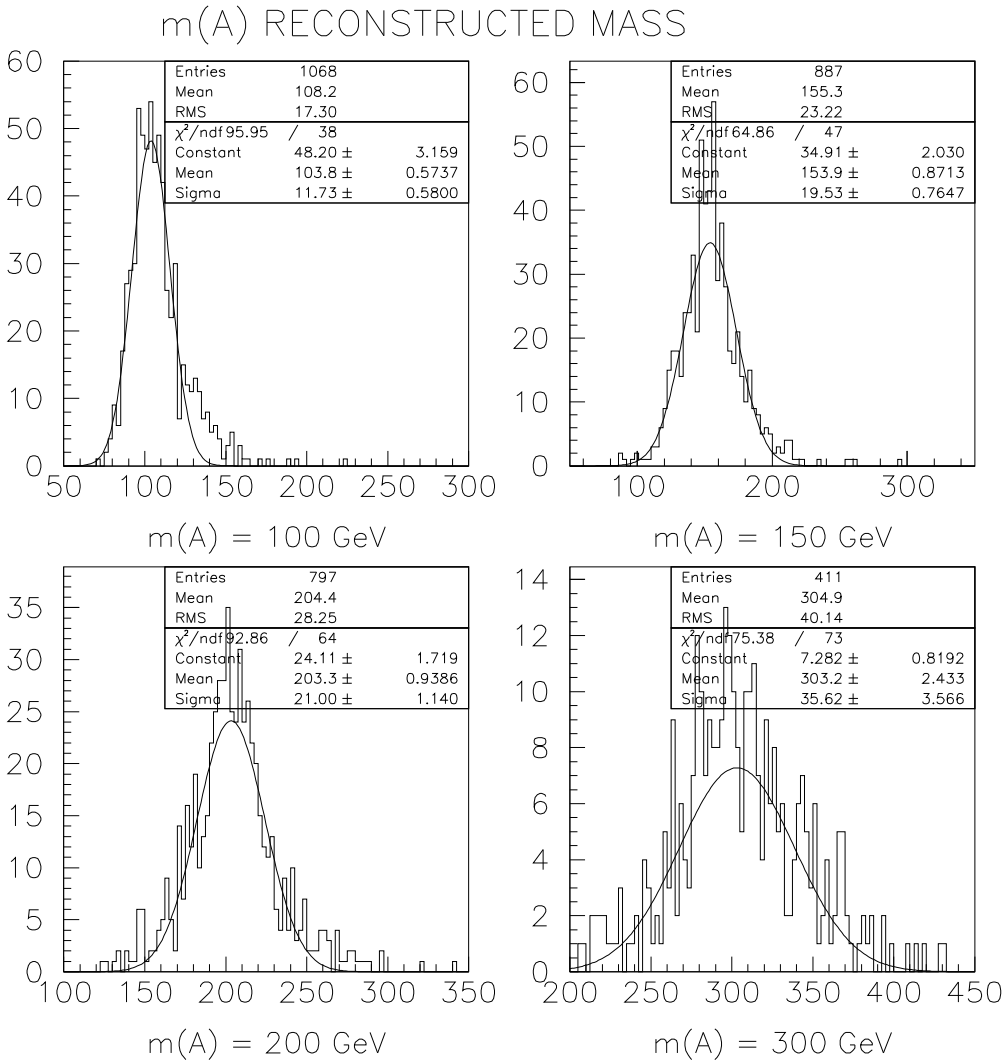

Figure 7: *Reconstructed $m_{\tau\tau}$ for m_A=100, 150, 200 and 300 GeV.*

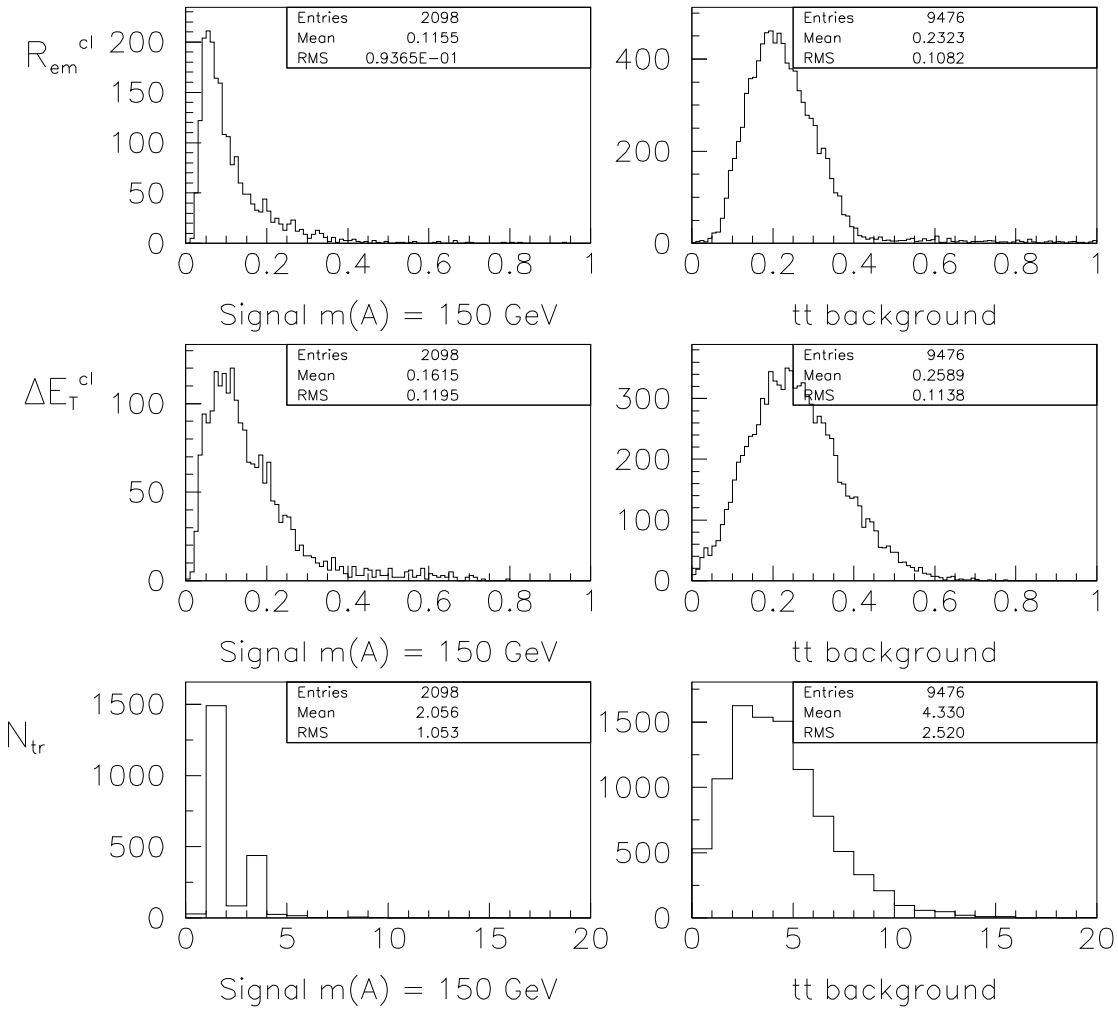

Figure 8: *τ identification distributions for τ's from A (m_A=150 GeV) ($p_T > 40$ GeV) and for the jets from the $t\bar{t}$ background ($p_T > 40$ GeV).*

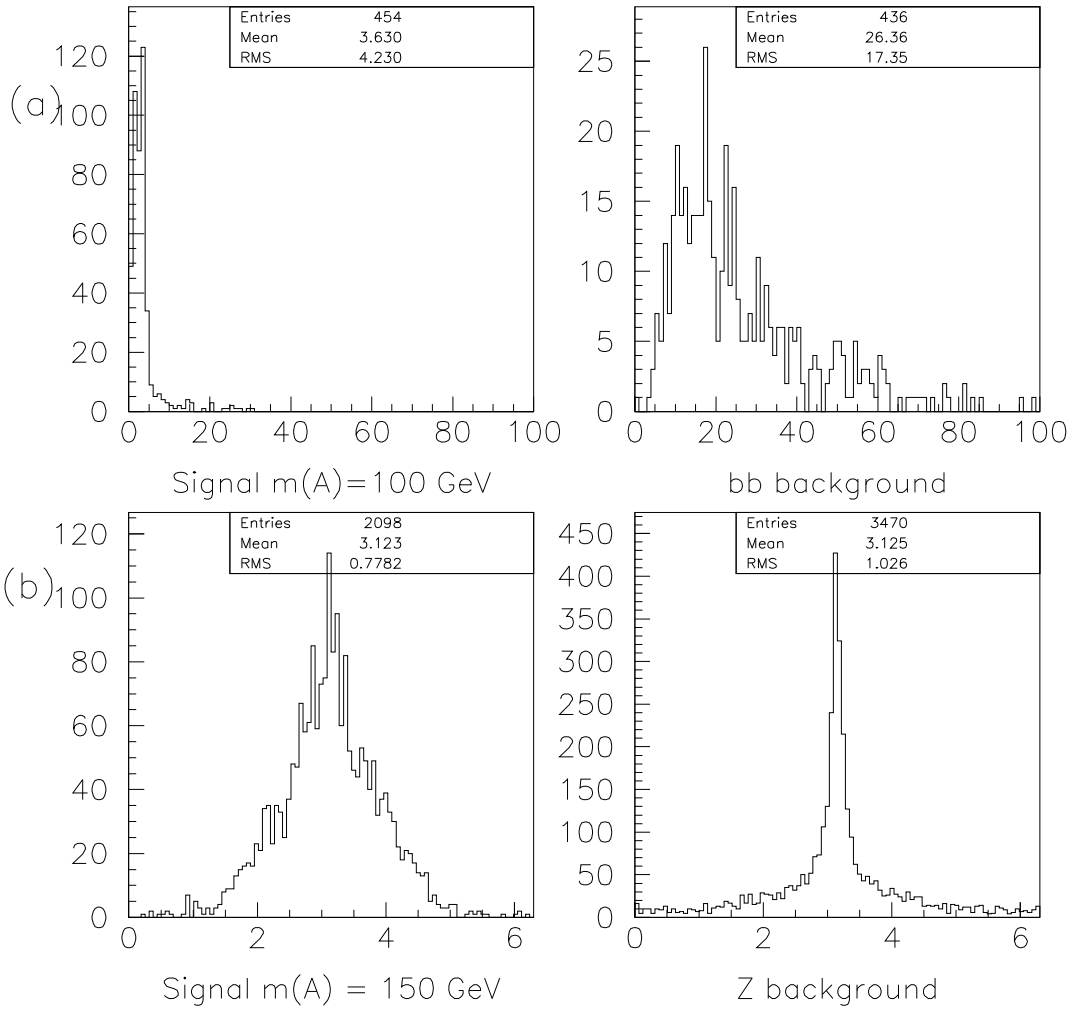

Figure 9: *(a) E_T in a window of half-width = 0.6 centered around the lepton (p_T >24 GeV) for m_A=100 GeV and b $\bar{b}$ background; (b) $\Delta\phi(jet-\mu)$ for m_A=100 GeV and Z^0 background.*

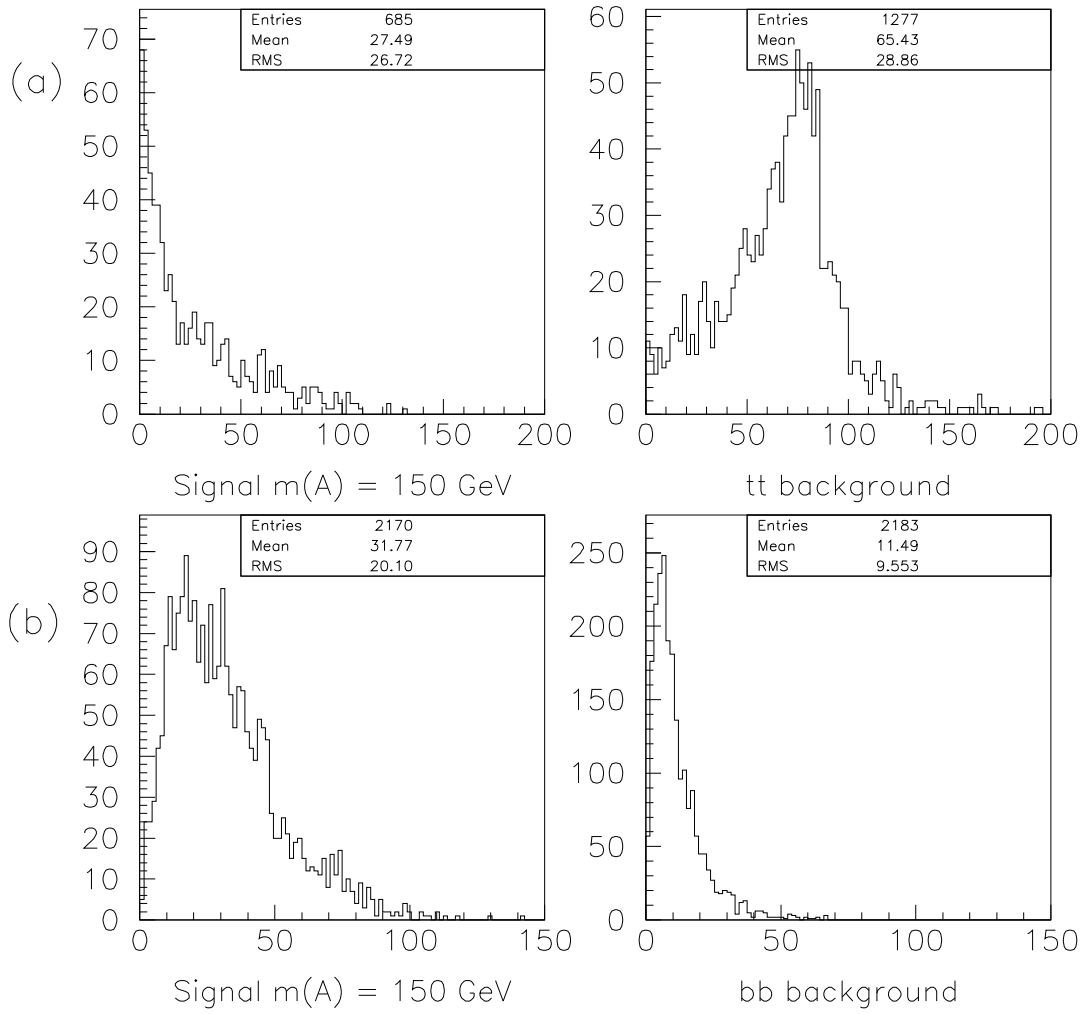

Figure 10: *(a) $m_T(\mu - p_T^{miss})$ for signal ($m_A = 150 GeV$) and $t\bar{t}$ background; (b) p_T^{miss} for signal ($m_A = 150$ GeV) and $b\bar{b}$ background.*

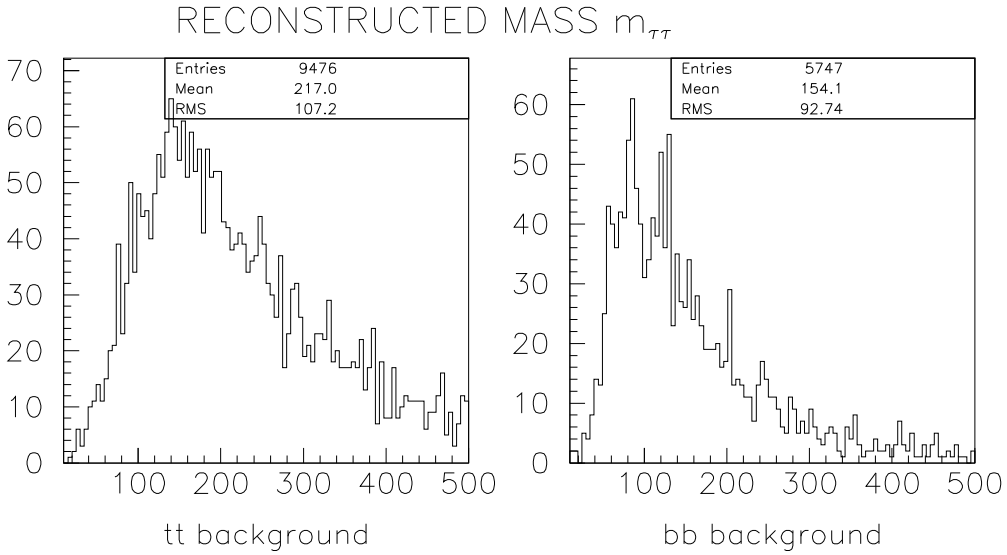

Figure 11: *Reconstructed mass $m_{\tau\tau}$ for $t\bar{t}$ and $b\bar{b}$ backgrounds.*

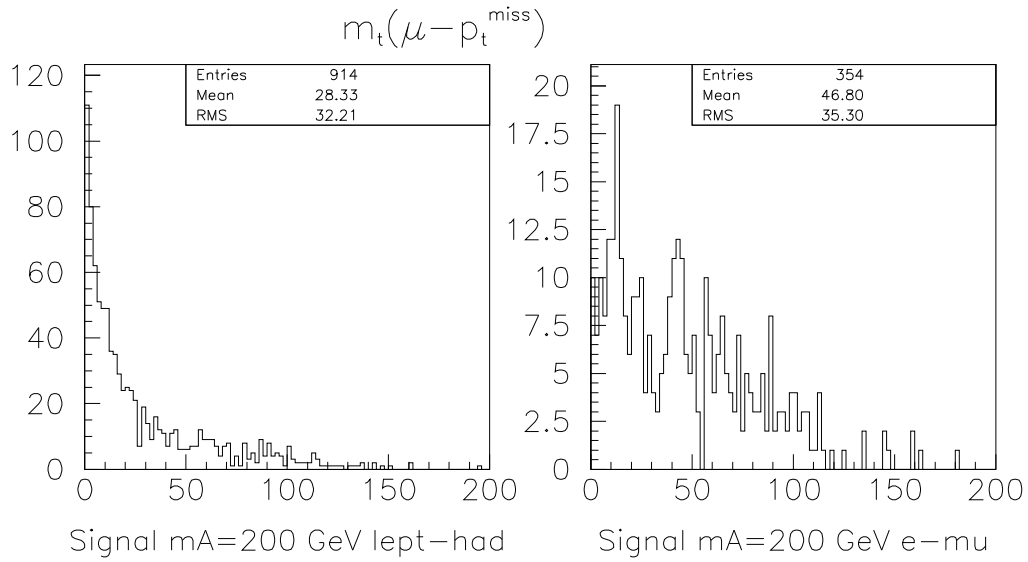

Figure 12: *$m_T(\mu - p_T^{miss})$ for m_A= 200 GeV in the lepton-hadron and $e - \mu$ channel.*

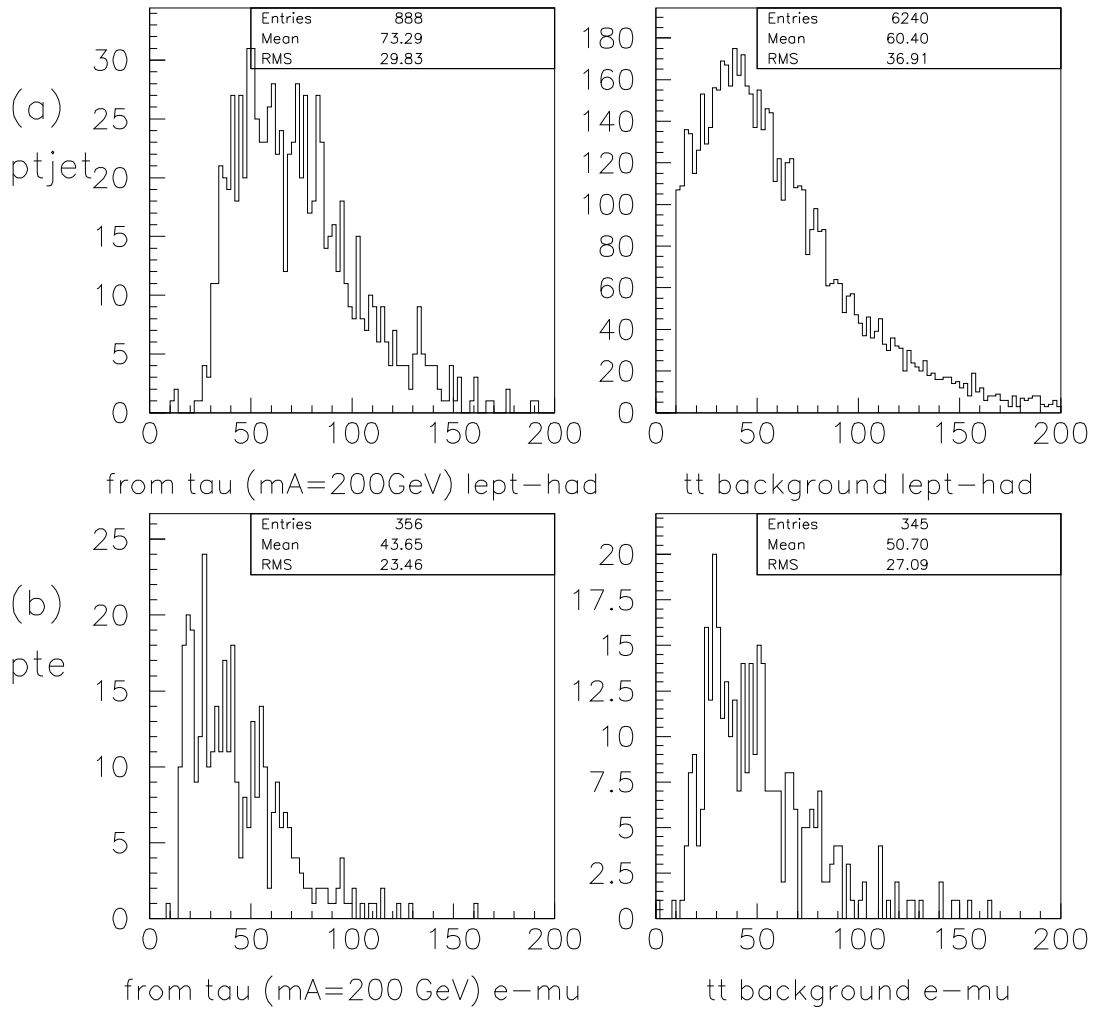

Figure 13: *(a) $E_T{}^{jet}$ from τ in A, m_A=200 GeV and in $t\bar{t}$ background in the lepton-hadron channel; (b) p_T^e from τ in A, m_A=200 GeV and in $t\bar{t}$ background in e - μ channel.*

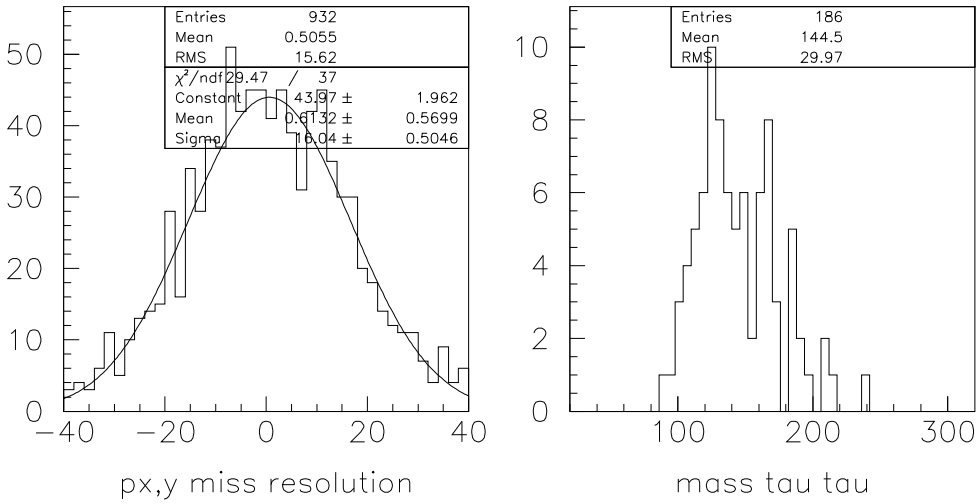

Figure 14: p_x^{miss} *and* p_y^{miss} *resolution and* $m_{\tau\tau}$ *resolution at* $10^{34}\ cm^{-2}s^{-1}$

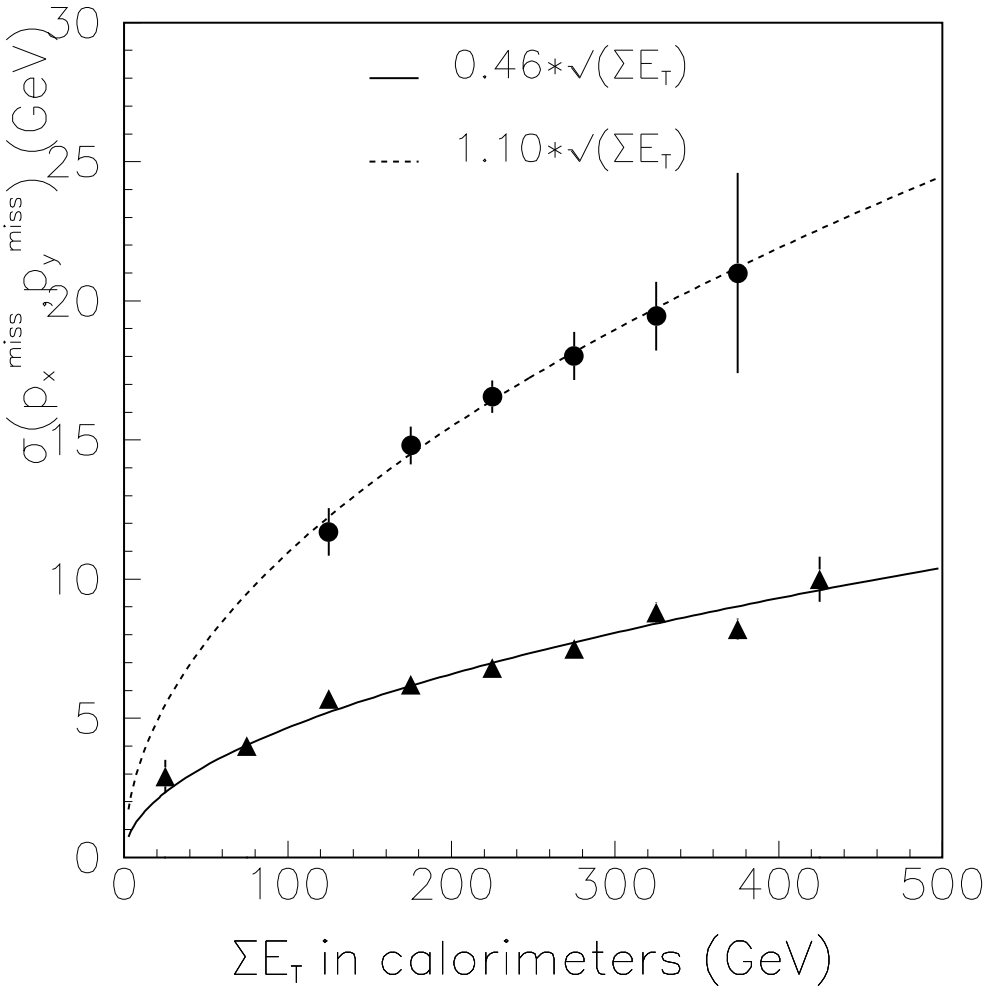

Figure 15: *ATLAS detector* p_T^{miss} *resolution vs* ΣE_T *at* 10^{33} $cm^{-2}s^{-1}$ *and* 10^{34} $cm^{-2}s^{-1}$.

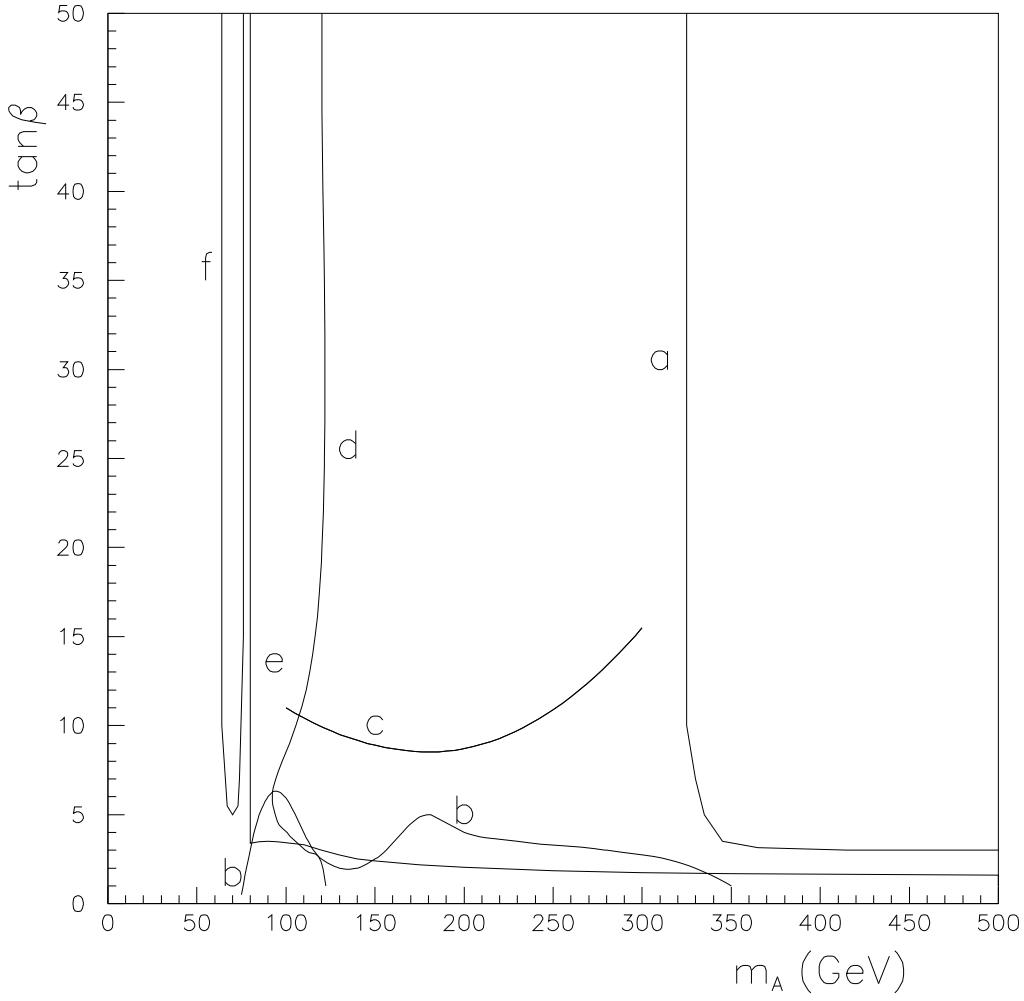

Figure 16: *The 5σ-discovery contour curves in the (m_A, $\tan\beta$) plane for various MSSM Higgs signals. The contour curves for (a) the $h \to \gamma\gamma$ channel, (b) the $H \to ZZ \to 4\ell$ channel, and (f) the $H \to \gamma\gamma$ channel, are shown for an integrated luminosity of 10^5 pb^{-1}. The contour curves for (c) the $A \to \tau\tau$ channel, and (d) the $t \to bH^+$ channel are shown for an integrated luminosity of 10^4 pb^{-1}. Curve (e) corresponds to the sensitivity expected at LEP2 for a centre-of-mass energy of 190 GeV.*